Experimental Study on the Plastic Rotation Capacity of Reinforced High Strength Concrete Beams

Man-Young Ko[1], Sang-Woo Kim[2], and Jin-Koo Kim[2]

1)Dept. of Architectural Design, Cheju Halla College, Jeju, Korea

2) Dept. of Architectural Engineering, Sungkyunkwan University, Suwon, Korea

Abstract. This paper describes an experimental study on the plastic rotation capacity of reinforced high strength concrete beams. Thirty-six beams with various compressive strengths of concrete, tensile reinforcement ratios, compressive reinforcement ratios, and patterns of loading (1 point loading and 2 points loading) were tested to evaluate the plastic rotation capacity, extreme fiber concrete compressive strain and equivalent plastic hinge length, etc. The same quantities were also obtained from numerical analysis and compared with experimental data. According to the results, the yield curvatures obtained from experiments turned out to be quite close to those obtained from theoretical approach. However, the experimental results for ultimate curvatures were significantly larger than those of theoretical prediction based on the assumption of ε_{cu}=0.003. Based on these observations, a new formula for ultimate strain is proposed for high strength concrete beams. Also the test results for plastic rotation capacity were found to be closer to those obtained using moment-curvature relationship considering tension stiffening of concrete and shear effect than those obtained using equivalent plastic hinge length. This substantiates that for accurate evaluation of plastic rotation capacity the consideration of tension stiffening of concrete and shear effect is most important.

Key words : Reinforced High Strength Concrete Beam, Plastic Rotation Capacity, Ultimate Concrete Compressive Strain of Extreme Fiber, Equivalent Plastic Hinge Length

1. Introduction

The use of high strength concrete has the advantage of reducing member size and story height. However the tendency of brittle behavior in high strength concrete beams has been left as a problem to be solved. In this sense the evaluation of the plastic rotation capacity of high strength reinforced concrete members is an important topic. However, the plastic rotation capacity is a complex issue, mainly because of interaction of the various parameters such as materials, member geometry, loading conditions, etc. Due to the large variation of these factors experimental results from previous research show significant scatter of the measured values of rotation capacity. The readers can refer to references [9, 15] for further information about the research related to the plastic rotation capacity of reinforced concrete beams.

As can be found in the references, a lot of research has been carried out in the field of flexural behavior of normal strength concrete structures. However, a further research is still needed for application on high strength concrete structures. In this research an available plastic hinge capacity of high strength concrete beams is investigated based on both experimental results and theoretical approach considering tension stiffening and shear effect.

2. Flexural deformation of members

From equilibrium conditions of a beam subjected to bending moment the moment-curvature relationship can be obtained as follows [2, 7, 10]:

$$M = \frac{b}{\varphi}\int_0^{\varepsilon_c} f_c\,\varepsilon_c\,d\varepsilon \;+\; A_s' f_s'\left(\frac{\varepsilon_c}{\varphi d} - k'\right)d \;+\; A_s f_s\left(1 - \frac{\varepsilon_c}{\varphi d}\right)d \tag{1}$$

where ε_c is the strain of concrete, and k' is the ratio of depth to centroid of compression bars and effective depth. The curvatures at first yield of tension steel and at ultimate load of reinforced concrete member are expressed as [9]:

$$\varphi_y = \frac{f_y / E_s}{d(1-k)} \tag{2}$$

$$\varphi_u = \varepsilon_{cu} / c \tag{3}$$

where ε_{cu} is the ultimate compressive strain of concrete, and c is the depth of the neutral axis at ultimate.

The rotation and deflection between any two points A and B of a member can be obtained by integrating the curvatures along the member length [9].

$$\theta_{AB} = \int_A^B \varphi \, dx \tag{4a}$$

$$\Delta_{AB} = \int_A^B x \, \varphi \, dx \tag{4b}$$

where dx is a length of an element of the member, and x is the distance of element dx from A.

2.1 Deformations obtained from moment-curvature relationships

The above equations are generalizations of the moment-area theorems, and apply whether elastic or plastic curvatures are involved. The equations can be used to calculate the rotations and deflection of members when their moment-curvature relationships and the distribution of bending moment are known. However, such an approach ignores the effect of the increase in stiffness of members due to tension carried by the concrete between the cracks, as well as the additional deformations caused by diagonal tension cracks due to shear.

2.1.1 Tension stiffening effect of concrete

The concrete subjected to tensile force is generally neglected in analysis when it is cracked. In reality, however, some of the tensile force in reinforcing steel is transferred to concrete, increasing tensile strength of steel. This effect, which is called tension stiffening effect, is considered in ACI code by the effective moment of inertia determined between cracked and uncracked section. CEB uses the simplified stress-strain relationship shown in Fig. 1 for reinforcing steel to take into account the tension stiffening effect of concrete. In this study, the tension stiffening effect is taken into account using CEB approach [4].

2.1.2 Shear effect

Fig. 2 shows the effect of shear force in the computation of plastic deformation. It is denoted in Fig.

2 that the plastic rotation capacity is contributed from two parts; the rotation due to bending (region A in Fig. 2(c)) which can be computed from moment-curvature relationship, and that due to shear effect which is accompanied by change in tensile force line (region B). The length of plastic area caused by tension due to shear can be obtained considering the angle of crack. In this study the test results are compared with the analytical model for length of plastic area (Naples model [15]).

2.2 Deformations obtained from the length of equivalent plastic hinge

The actual curvature distribution at ultimate stage can be idealized into elastic and inelastic regions (Fig. 3). The elastic contribution to rotation and deflection may be calculated from Equation (4). The shaded area represents the inelastic curvature which causes plastic rotation occurring in addition to the elastic rotation at the ultimate stage. The region of inelastic curvature, where the bending moment exceeds the yield moment of the section, is spread over a certain length of beams. In this region the curvature fluctuates because of the increased rigidity of the member between the cracks. However, for convenience, the inelastic area at the ultimate stage can be replaced by an equivalent rectangle of height $(\varphi_u - \varphi_y)$ and width l_p, having the same area as the actual inelastic curvature distribution [9]. Hence the plastic hinge rotation to one side of the critical section can be written as:

$$\theta_p = (\varphi_u - \varphi_y) l_p \tag{5}$$

The rotation and deflection between two points A and B when the ultimate moment is reached at the critical section are as follows assuming an idealized inelastic curvature distribution:

$$\theta_{AB} = \theta_e + \theta_p = \varphi_y \frac{1}{2} + (\varphi_u - \varphi_y) l_p \tag{6}$$

$$\Delta_{AB} = (\frac{\varphi_y l}{2} \frac{2l}{3}) + (\varphi_u - \varphi_y) l_p (l - \frac{l_p}{2}) \tag{7}$$

The length of equivalent plastic hinge l_p can be obtained from experiment and the following equations were suggested by various researchers [9]:

$$l_p = 0.8 K_1 K_3 (\frac{z}{d}) c \quad (8a)$$

$$l_p = 0.5d + 0.32\sqrt{d}\,(\frac{z}{d}) \quad (8b)$$

$$l_p = 0.5d + 0.05z \quad (8c)$$

$$l_p = 0.25d + 0.075z \quad (8d)$$

where K_1 = 0.7 for mild steel or 0.9 for cold-worked steel, K_3 = 0.6 when f_c' = 35.2 MPa or 0.9 when f_c' = 11.7 MPa assuming f_c' = 0.85 × cube strength of concrete, z = distance of critical section to the point of contraflexure (cm), d = effective depth of member (cm), and c = the neutral axis depth at the ultimate moment (cm). In this research Equation (5) is used to compute the plastic hinge rotation, and the results are compared with those obtained from Equation (4a) considering the effect of tension stiffening and shear on the moment-curvature relationship.

3. Flexural test of high strength concrete beams

3.1 Test specimens

A total of 36 rectangular reinforced concrete beams made of ordinary portland cement (Type I) were prepared for the test. The maximum diameter of the coarse aggregate used in the specimens was 13 mm, and the specific gravity and fineness modulus were 2.65 and 6.46, respectively. The specific density and fineness modulus of fine aggregates were 2.64 and 2.74, respectively. Light gray density microsilica with a specific gravity of 2.2 and a specific surface area of 20m^2/g was used, and the melamine type high range water reducer was added to realize high strength and high flowability. The details of concrete mix design are given in Table 1.

The compressive strength tests of concrete (100 × 200mm cylinders) were carried out in accordance with ASTM C39. The average concrete compressive strengths of beams with design strength of 60, 70, and 80 MPa were found to be 66.6, 70.8 and 82.1 MPa, respectively, and the average elastic modulus were 31.2, 34.6 and 36.4 GPa, respectively. The tensile tests of reinforcing bars were

conducted following ASTM A47 guideline. The properties of deformed bars are given in Table 2.

All beams were doubly reinforced and provided with shear reinforcement. In the first phase of experiments the effects of concrete compressive strength (60 and 80 MPa), ratio of tensile reinforcement (ρ =0.30, 0.50, 0.65, and 0.75 ρ_b), and loading type (one point and two points loading) were studied. In the second phase the compressive strength was fixed to 70 MPa, and the effects of tensile reinforcement (ρ =0.30, 0.65, 0.95, 1.32 ρ_b), compressive reinforcement (ρ' / ρ = 0.0, 0.15, 0.3, 0.5, 0.75), and loading type (one point and two points) were investigated. The shear reinforcements were placed at the interval of $d/2$ to prevent the shear failure, and the shear span ratio (a/d=4.0, 5.8, 4.5, 6.0) was determined so that flexural failure occurs.

The size, shape and reinforcement details of the test specimen, along with the location of the strain gages, are shown in Fig. 4. Table 3 lists the concrete compressive strengths, reinforcing bars used, reinforcement ratios, loading types, and length of shear span of each test specimen. The notations for beam designation are as follows:

$$7 - 75^{15} - 1$$

where 7 : compressive strength of concrete (70 MPa), 75 : tensile reinforcement ratio (ρ =0.75 ρ_b), 15 : double reinforcement ratio (ρ' =0.15 ρ), and 1: loading type (1-point loading).

3.2 Test procedure and results

The test specimens were simply supported and were subjected to one and two-point loads, as shown in Fig. 5. The distance between the two-point loads was kept constant at 460 mm in the first phase of experiments (6 and 8 series beams), and at 450 mm in the second phase (7 series beams). The beam midspan deflection was measured by a LVDT, and the strain gages were attached to several locations to record the strain of concrete and reinforcing bars. The load was applied until the crushing in the compressed region of concrete occurred.

The test results are shown in Fig. 6 and Table 4, which demonstrate that the flexural strength

increases as the concrete compressive strength and tensile steel ratio increase, and that the displacement at the first yield decreases as the compression steel ratio increases. The ductility tends to be larger for the beams subjected to one-point load than for those under two-point load. It also can be noticed from the figures that the sustained load after the failure decreases more slowly in the one-point load experiments. During the test it was observed that the vertical flexural cracks occurred near the loading points and in the constant-moment region, whereas the diagonal cracks were formed between the loading points and the supports of the beams before final failure of the beams due to crushing of concrete occurred. It was also observed that as the tensile and compression steel ratios increased less vertical cracks propagate and more diagonal cracks formed (Fig. 7).

4. Discussion of results

4.1 Curvature and ultimate concrete compressive strain of extreme fiber

The curvatures at the first yield of the tension steel and at failure measured from the tests are presented in Table 4. Also given are the results obtained from the theoretical approach. According to the test results the normal strain at the locations of tension steel, compression steel, and the extreme fiber at compression side did not vary linearly. However, for convenience, the curvature was estimated linearly based on the strain of tension steel and concrete compressive strain of extreme fiber. The theoretical value at the first yield of the tension steel was computed using Equation (2) assuming linear elasticity of the material. The curvatures at the ultimate load were computed by Equation (3) using ε_{cu} =0.003, and the depth of the neutral axis at the ultimate state was obtained using the MacGregor stress block [5, 6].

The comparison of the yield curvatures obtained from experiments and theory shows that their difference is less than 10 % in most of the cases (Table 4, Fig. 8*a*). The comparison of curvatures at the ultimate load, however, provides quite different results (Fig. 8b). The test results are about 1.7 to 2 times greater than those obtained from Equation (3). The reason for this overestimation is that the depth of the neutral axis at the ultimate load obtained using MacGregor stress block is based on ε_{cu} to estimate the

theoretical value of the curvature at the ultimate load.

The average value and the standard deviation of the ultimate concrete compressive strain at the extreme fiber are 0.0040~0.0044 and 0.00048~0.00073, respectively, depending on the concrete compressive strength. The lower limit of the 90 % confidence range is 0.0033. It can be seen in Figs. 9 and 10 that ε_{cu} generally decreases as the compressive strength of concrete and tensile reinforcement ratio increase, and increases as the compression steel increases. The dotted lines in those figures represent the lower boundary of the 90 % confidence range. Based on the lower limit the following formula is proposed for the ultimate concrete compressive strain of the extreme fiber:

$$\varepsilon_{cu} = 0.003 + 1.44\frac{1}{(f_c')^2} + 0.00054\left(\frac{\rho'}{\rho}\right) \tag{9}$$

where f_c' is the compressive strength of concrete (60～80 MPa).

4.2 Equivalent length of Plastic hinge

It is generally agreed that the inelastic rotations are concentrated over a length called "plastic hinge length" where $M_y \le M \le M_u$. Plastic hinge length is dependent on the shape of the bending moment diagram at the ultimate stage, and is also affected by the distance between points of contraflexure, distance between support and the point of contraflexure, reinforcement ratio, and the compressive strength of concrete [9].

Fig. 11 presents the plastic hinge lengths obtained from the test results of one-point loading and from the equations proposed by various researchers (Equation (8)). It can be noticed in Table 5 that the deflections at ultimate state ($\Delta_{u,cur.}$) obtained from the moment area of the curvature diagram are reasonably close to the measured values using LVDT, being 86 % of the measured value in average. The plastic hinge length was computed by equating the area enclosed between the curvature diagrams at the first yield and those at the ultimate state with the equivalent rectangle of width lp and height ($\varphi_u - \varphi_y$) having the same area.

In the experiments the strains were measured only at one half of the beams expecting symmetric behavior. But for two-point loading tests, the plastic hinge length was not obtained because of unsymmetric behavior of some test specimens after yielding. For one-point loading tests, no dominant relationship between concrete compressive strength or reinforcement ratio and the plastic hinge length could be observed as shown in Fig. 11(a), which presents the experimental data for equivalent plastic hinge length and the predictions from the four formulae presented before (Equation (8)). The plastic rotation θ_p obtained from the formulae utilizing the ε_{cu} proposed in this research (Equation (9)) is shown in Fig. 11(b). The formula of Corley was omitted because of its too much overestimation. From the comparison the Mattock's formula turned out to predict the experimental data most closely.

The deflections using Equation (7) and the proposed equations for the ultimate concrete compressive strain of the extreme fiber and equivalent length of plastic hinge correspond to 68% in average of those measured from LVDT (Table 5). This difference is considered to have occurred because the proposed equation for ε_{cu} was based on the lower limit of the 90 % confidence range. Therefore the proposed equivalent plastic hinge length is conservative enough to ensure safety.

4.3 Rotation capacity of plastic hinge

4.3.1 Rotation of plastic hinge obtained from moment-curvature relationships

Table 6 presents the experimental data and analysis results of the plastic hinge rotation. The analytical results were computed from the moment-curvature relationship (Equation (1)) and the equivalent length of plastic hinge (Equation (5)). In Table 6, the analytical results obtained by considering only the bending effect in Equation (1) are named as FL, in which the ascending and descending stress-strain curve of concrete proposed by Collins [12] and Attard et al. [1], was used in addition to the assumption of the ultimate strain of ε_{cu}=0.003 (Fig. 12(a)). In the results FL+TSE+SE the tensile strength of concrete and the effect of shear were considered as well as bending. The length of plastic area (l_v) was assumed to be kd based on the Naples model [15]. The results are plotted in Fig.

12(b). The comparison shows that the rotation capacity of beams obtained from experiments is better predicted by considering tension stiffening of concrete and shear effect. However, the experimental results of rotation capacity of beams subjected to one-point load are 2.43 times in average underestimated by the analysis. Therefore it can be concluded that for one-point loading case the length of plastic area was somewhat underestimated.

From Fig. 7 the average inclination of the cracks from vertical axis was estimated to be 37.7°, and at the midspan it was observed that the inclined shear-punching cracks started at about $1.55kd$ from the extreme compressive fiber. Based on these observations the length of the plastic area is proposed as $l_v = 1.2kd$ for more reasonable estimation of the rotation capacity of the plastic hinge. The plastic rotation capacity predicted by the proposed method, $\theta_{p,\,pro}$, is given in Table 6 and is compared with experimental data in Fig. 12(c). For one-point loading case the average and standard deviation of the experimental data turned out to be 1.73 and 0.313, respectively, and the limit of the 90% confidence was 1.21～2.24. Therefore the plastic rotation capacity predicted by the proposed approach provides a conservative result.

4.3.2 Plastic rotation capacity based on plastic hinge length

The plastic rotation capacity of the beams computed based on the ultimate concrete compressive strain of extreme fiber and the plastic hinge length proposed in this research, $\theta_{p,\,lp}$, is given in Table 6, and is compared with test results in Fig. 12 (d). For one-point loading the average value is 2.08, which is larger than the rotation computed by using moment-curvature relationship ($\theta_{p,\,pro.}$). This difference seems to be due to the tension stiffening effect of concrete and shear deformation. Therefore an appropriate consideration of these effects is necessary for precise evaluation of the plastic rotation capacity of high strength concrete beams.

5. Conclusions

In this research, an experimental study for plastic rotation capacity of reinforced high strength

concrete with compressive strength ranging from 60~80 MPa has been conducted, and the results are summarized as follows:

(1) According to the experimental results, the differences of the yield curvatures obtained from experiments and from theory are about 10 % in average. However, the theoretical estimation of the ultimate curvatures based on the assumption of ε_{cu} =0.003 underestimates the test results. For more reasonable estimation of ultimate curvature, a new equation for the ultimate concrete compressive strain of extreme fiber was proposed based on the lower limit of the 90% confidence.

(2) The plastic rotation capacity of high strength concrete beams obtained from the tests was better predicted by the moment-curvature relationship considering tensile strength of concrete and shear effect than by using the equation of equivalent plastic hinge length. This observation demonstrates the importance of the concrete tensile strength and the shear deformation in plastic rotation of high strength concrete beams.

(3) The plastic rotation capacity obtained from one-point loading tests was 1.73 times in average higher than that obtained from proposed analytical method based on the moment-curvature relationship considering tensile strength of concrete and shear effect. Therefore the proposed method provides conservative prediction of the plastic rotation capacity of high strength concrete beams.

Reference

[1] Attard, M. M. and Stewart, M. G., 'A Two Parameter Stress Block for High-Strength Concrete', *ACI Structural Journal* **95** (3) (1998) 305-317.

[2] Carreira, D. J. and Chu, K. H., 'The Moment-Curvature Relationship of Reinforced Concrete Members', *ACI Journal* **83** (1986) 191-198.

[3] CEB-FIP Working Group, 'High Performance Concrete - Recommended Extensions to the Model Code 90 - Research Needs', (1995).

[4] Comité Euro-International du Béton, 'CEB-FIP MODEL CODE 1990'.

[5] Ibrahim, H. H. H. and MacGregor, J. G, 'Modification of the ACI Rectangular Stress Block for High-Strength Concrete', *ACI Structural Journal* **94** (1) (1997) 40-48.

[6] Kim, S. W., Ko, M. Y. and Kim, Y. B., 'An Experimental Study on the Flexural Strength and Ductility Capacity of Reinforced High Performance Concrete Beams', *Journal of the Architectural Institute of Korea* **15** (7) (1999) 3-10.

[7] Angel L. Lazaro, III and Rowland Richards, 'Full-Range Analysis of Concrete Frames', *Journal of the Structural Division, ASCE* **99** (1973) 1761-1783.

[8] Nawy, E. G and Chen, B., 'Deformational Behavior of High Performance Concrete Continuous Composite Beam Reinforced with Prestressed Prisms and Instrumented with Bragg Grating Fiber Optic Sensors', *ACI Structural Journal* **95 (**1) (1998) 51-60.

[9] Park, R. and Pauley, T., 'Reinforced Concrete Structures', (John Wiley & Sons, 1975).

[10] Pfrang, E. O., Siess, C. P. and Sozen, M. A., 'Load-Moment-Curvature Characteristic of Reinforced Concrete Cross Sections', *ACI Journal* **61** (7) (1964) 763-778.

[11] Placas, A., Regan, P. E. and Baker, A. L. L., 'Shear Failure of Reinforced Concrete Beams', *ACI Journal* **68** (1971) 763-773.

[12] Rangan, B. V. and Warner, R. F., 'Large Concrete Buildings', (Longman Group Limited, 1996) 158-182.

[13] Scott, R. H., 'Behavior of High Strength Concrete Beams', *Proceedings of Third CANMET/ACI International Conference, Malaysia,* (1997) 119-133.

[14] Swamy, R. N. and Al-Ta'an, S. A., 'Deformation and Ultimate Strength in Flexure of Reinforced Concrete Beams Made with Steel Fiber Concrete', *ACI Journal* (1981) 395-405.

[15] CEB Task Group 2.2, 'Ductility of Reinforced Concrete Structures', (CEB, 1998).

[16] Wang, P. T., Shah, S. P. and Naaman, A. E., 'Stress-Strain Curves of normal and Lightweight Concrete in Compression', *ACI Journal* (1978) 603-611.

Captions for tables

Table 1 – Mix proportions

Table 2 – Properties of the deformed bars

Table 3 – Properties of test beams

Table 4 – Summary of test results

Table 5 – Comparison of experimental and theoretical results for deflection of specimens

Table 6 – Comparison of experimental and theoretical results for plastic rotation capacity of test beams

Table 1 – Mix proportions

Mix (MPa)	W/C (%)	S/A (%)	Unit volume weight (kg/m^3)				Admixture (kg/m^3)	
			W	C	S	G	S.F	S.P
60	30	38	167.0	530	629	1026	26.5	21.2
70	29	38	169.3	530	629	1026	53.0	21.2
80	27	39	169.3	570	629	1026	57.0	22.8

Table 2 – Properties of the deformed bars

Bar size	Area (cm^2)	Yeild strengh (MPa)	Tensile strength (MPa)	Elastic modulus (GPa)
D10	0.71	406	608	175
D13	1.27	413	579	200
D16	1.99	443	640	172
D19	2.87	419	615	174
D22	3.87	385	588	172

Table 3 – Properties of test beams				
Beams	f_c' (MPa)	Tension steel		$\frac{\rho'}{\rho}$
		Number of bar	$\frac{\rho}{\rho_b}$	
6-30-1	66.6	2-D13, 1-D10	0.33	0.44
8-30-1		3-D13	0.34	0.37
6-50-1		2-D16, 1-D13	0.54	0.33
8-50-1		3-D16	0.54	0.24
6-65-1	82.1	2-D19, 1-D10	0.66	0.22
8-65-1		2-D19, 1-D16	0.70	0.18
6-75-1		2-D19, 1-D16	0.79	0.18
8-75-1		2-D22, 1-D13	0.81	0.16
6-30-2	66.6	2-D13, 1-D10	0.33	0.44
8-30-2		3-D13	0.34	0.37
6-50-2		2-D16, 1-D13	0.54	0.33
8-50-2		3-D16	0.54	0.24
6-65-2	82.1	2-D19, 1-D10	0.66	0.22
8-65-2		2-D19, 1-D16	0.70	0.18
6-75-2		2-D19, 1-D16	0.80	0.18
8-75-2		2-D22, 1-D13	0.81	0.16
$7\text{-}32^{00}\text{-}2$	70.8	2-D16 1-D10	0.29	0.00
$7\text{-}32^{30}\text{-}2$				0.30
$7\text{-}62^{00}\text{-}2$		1- D22 2-D19	0.59	0.00
$7\text{-}62^{15}\text{-}2$				0.15
$7\text{-}62^{30}\text{-}2$				0.30
$7\text{-}62^{50}\text{-}2$				0.50
$7\text{-}62^{75}\text{-}2$				0.75
$7\text{-}92^{00}\text{-}2$		3-D22 2-D13	0.87	0.00
$7\text{-}92^{15}\text{-}2$				0.15
$7\text{-}92^{30}\text{-}2$				0.30
$7\text{-}92^{50}\text{-}2$				0.50
$7\text{-}92^{75}\text{-}2$				0.75
$7\text{-}132^{00}\text{-}2$		5-D22	1.19	0.00
$7\text{-}132^{15}\text{-}2$				0.15
$7\text{-}132^{30}\text{-}2$				0.30
$7\text{-}132^{50}\text{-}2$				0.50
$7\text{-}132^{75}\text{-}2$				0.75
$7\text{-}62^{00}\text{-}1$		1-D22 2-D19	0.59	0.00
$7\text{-}62^{15}\text{-}1$				0.15
$7\text{-}62^{30}\text{-}1$				0.30
Stirrup : 6 and 8 series beams : D10 @60mm 7 series beams : D10 @70mm				

Table 4 – Summary of test results

Beams	P_y (kN)	Δ_y (mm)	φ_y ($\times 10^{-4}$ rad/cm)			P_u (kN)	Δ_u (mm)	φ_u ($\times 10^{-4}$ rad/cm)			ε_{cu}	$\frac{\Delta u}{\Delta y}$	$\frac{\varphi u}{\varphi y}$
			Exp.	*Cal.*	$\frac{Exp.}{Cal.}$			*Exp.*	*Cal.*	$\frac{Exp.}{Cal.}$			
6-30-1	45.49	5.9	3.48	3.75	0.93	52.55	15.3	16.27	12.20	1.33	0.0046	2.59	4.68
6-50-1	76.47	7.2	4.60	4.02	1.14	81.27	19.6	15.94	7.96	2.00	0.0037	2.72	3.47
6-65-1	88.73	8.1	4.56	3.56	1.28	93.43	16.7	13.47	7.39	1.82	0.0033	2.06	2.95
6-75-1	103.82	8.5	4.95	4.19	1.18	108.04	11.5	12.62	6.09	2.07	0.0044	1.35	2.55
6-30-2	67.45	6.8	3.33	3.67	0.91	81.86	30.3	15.29	11.76	1.30	0.0048	4.46	4.59
6-50-2	113.82	9.0	4.49	4.22	1.06	122.25	22.5	14.11	8.29	1.70	0.0045	2.34	3.14
6-65-2	130.10	9.2	4.44	3.82	1.16	136.47	17.7	13.20	7.54	1.75	0.0043	1.92	2.76
6-75-2	151.76	10.6	4.88	4.44	1.10	153.92	12.9	9.51	6.15	1.55	0.0039	1.22	1.95
Ave.					1.10					1.69	0.0042		
S.D*					0.12					0.27	0.00048		
8-30-1	56.76	8.08	4.31	3.64	1.18	64.61	19.65	18.8	11.28	1.67	0.0051	2.43	4.36
8-50-1	93.04	8.92	4.34	4.06	1.07	98.24	14.32	17.3	8.11	2.13	0.0041	1.61	3.99
8-65-1	97.16	8.18	4.12	3.76	1.10	110.69	11.56	12.5	6.21	2.01	0.0039	1.41	3.03
8-75-1	110.10	9.57	5.00	4.77	1.05	122.55	15.69	16.1	5.98	2.69	0.0050	1.64	3.22
8-30-2	76.76	8.47	3.47	2.99	1.16	85.59	24.51	16.2	11.19	1.45	0.0041	2.89	4.67
8-50-2	119.41	9.36	3.85	4.06	0.95	128.33	12.17	11.3	8.11	1.39	0.0028	1.30	2.94
8-65-2	151.67	12.49	4.79	4.50	1.06	156.86	16.36	13.9	6.48	2.15	0.0035	1.31	2.90
8-75-2	147.06	10.37	4.15	3.95	1.05	155.69	12.53	10.5	5.98	1.76	0.0034	1.21	2.53
Ave.					1.08					1.91	0.0040		
S.D					0.067					0.40	0.00073		
7-32^{00}-2	88.63	8.90	2.70	2.79	0.97	98.92	23.00	13.73	11.72	1.17	0.0044	2.58	5.09
7-32^{30}-2	92.65	8.30	2.77	2.80	0.99	106.18	34.40	14.42	11.76	1.23	0.0038	4.14	5.21
7-62^{00}-2	147.25	11.69	3.64	3.32	1.10	161.67	24.60	16.78	6.45	2.60	0.0046	2.10	4.60
7-62^{15}-2	133.33	12.27	3.39	3.15	1.08	156.18	29.97	15.58	6.90	2.26	0.0046	2.44	4.59
7-62^{30}-2	147.35	11.01	3.13	3.21	0.98	172.45	35.35	17.35	7.28	2.38	0.0053	3.21	5.54
7-62^{50}-2	154.41	9.10	2.99	2.77	1.08	164.41	20.10	14.07	8.45	1.67	0.0043	2.21	4.71
7-62^{75}-2	153.82	9.70	2.92	2.63	1.11	164.22	22.00	13.19	8.15	1.62	0.0048	2.27	4.52
7-92^{00}-2	220.69	15.21	3.34	3.23	1.03	230.49	21.24	3.92	4.12	0.95	0.0037	1.40	1.17
7-92^{15}-2	210.88	14.07	3.59	2.88	1.25	215.69	20.11	10.48	4.62	2.27	0.0051	1.43	2.92
7-92^{30}-2	225.88	13.68	3.81	3.71	1.03	231.57	19.30	14.18	5.03	2.82	0.0044	1.41	3.72
7-92^{50}-2	223.14	10.80	3.59	3.66	0.98	224.31	13.30	6.86	6.28	1.09	0.0033	1.23	1.91
7-92^{75}-2	223.82	10.70	3.10	2.88	1.08	229.80	19.70	10.75	6.54	1.64	0.0045	1.84	3.47
7-132^{00}-2	-	-	-	-	-	-	-	-	-	-	-	-	-
7-132^{15}-2	230.58	15.31	4.44	4.36	1.02	268.14	29.53	16.67	3.59	4.64	0.0053	1.93	3.75
7-132^{30}-2	235.59	14.29	4.59	4.18	1.10	259.90	18.18	10.49	4.12	2.55	0.0042	1.27	2.29
7-132^{50}-2	233.73	12.40	3.76	3.23	1.16	255.39	16.70	9.32	5.08	1.83	0.0043	1.35	2.48
7-132^{75}-2	236.08	11.10	3.96	3.70	1.07	257.84	17.60	15.51	6.34	2.45	0.0041	1.60	3.92
7-62^{00}-1	119.12	10.42	3.18	2.84	1.12	127.55	20.08	13.96	6.45	2.16	0.0046	1.93	4.39
7-62^{15}-1	115.69	10.24	3.22	3.15	1.02	127.35	18.11	13.31	6.90	1.93	0.0039	1.77	4.13
7-62^{30}-1	118.04	8.50	3.17	2.76	1.15	133.24	20.63	13.81	7.25	1.90	0.0048	2.43	4.35
Ave.					1.07					2.06	0.0044		
S.D					0.070					0.81	0.00051		

* Standard deviation

Table 5 – Comparison of experimental and theoretical results for deflection of specimens (Unit : cm)

Beams	$\Delta_{u,LVDT}$ *	$\Delta_{u,cur.}$ **	$\frac{\Delta_{u,cur.}}{\Delta_{u,LVDT}}$	$\Delta_{u,pro.}$ ***	$\frac{\Delta_{u,pro.}}{\Delta_{u,LVDT}}$
6-30-1	1.53	1.25	0.82	1.26	0.82
6-50-1	1.96	1.36	0.69	1.05	0.54
6-65-1	1.67	1.26	0.75	1.00	0.60
6-75-1	1.15	1.04	0.90	0.94	0.82
8-30-1	1.97	1.66	0.84	1.24	0.63
8-50-1	1.43	1.28	0.90	1.00	0.70
8-65-1	1.16	1.13	0.97	0.84	0.72
8-75-1	1.57	1.26	0.80	0.91	0.58
7-62^{00}-1	2.01	1.86	0.93	1.25	0.62
7-62^{15}-1	1.81	1.74	0.96	1.32	0.73
7-62^{30}-1	2.06	1.79	0.87	1.37	0.67
Ave.			0.86		0.68
S.D			0.084		0.088

* Displacement at ultimate state measured by LVDT

** Displacement at ultimate state obtained from curvature diagram

*** Displacement at ultimate state obtained from Eq. (7) using proposed ε_{cu} and plastic hinge length

Table 6 – Comparison of experimental and theoretical results for plastic rotation capacity of test beams (Unit : 10^{-2} rad)

Beams	Test results		Theoretical results using moment-curvature relationships									Theoretical results using l_p ***		
			FL*			FL+T.S.E+S.E**								
						Naples Model			Proposed					
	$\theta_{u,exp.}$	$\theta_{p,exp.}$	$\theta_{u,Flexure}$	$\theta_{p,Flexure}$	$\frac{\theta_{p,exp.}}{\theta_{p,Flexure}}$	$\theta_{u,Naples}$	$\theta_{p,Naples}$	$\frac{\theta_{p,exp.}}{\theta_{p,Naples}}$	$\theta_{u,pro.}$	$\theta_{p,pro.}$	$\frac{\theta_{p,exp.}}{\theta_{p,pro.}}$	$\theta_{u,lp}$	$\theta_{p,lp}$	$\frac{\theta_{p,exp.}}{\theta_{p,lp}}$
6-30-1	2.33	1.14	1.24	0.25	4.56	1.54	0.73	1.56	1.84	0.96	1.19	2.35	1.04	1.10
6-50-1	2.50	1.13	1.27	0.11	10.27	1.57	0.39	2.90	1.80	0.56	2.02	1.92	0.51	2.20
6-65-1	2.36	0.93	1.23	0.10	9.30	1.55	0.36	2.58	1.77	0.52	1.79	1.73	0.48	1.93
6-75-1	2.06	0.45	1.34	0.06	7.50	1.60	0.23	1.96	1.80	0.36	1.25	1.74	0.27	1.68
8-30-1	2.98	1.48	1.38	0.35	4.23	1.64	0.77	1.92	1.95	1.01	1.47	2.16	0.89	1.67
8-50-1	2.41	0.90	1.36	0.13	6.92	1.63	0.42	2.14	1.86	0.56	1.61	1.90	0.48	1.89
8-65-1	2.25	0.81	1.45	0.08	10.13	1.68	0.25	3.24	1.87	0.38	2.13	1.61	0.29	2.78
8-75-1	2.42	0.67	1.42	0.07	9.57	1.66	0.23	2.91	1.84	0.34	1.97	1.84	0.19	3.53
7-62^{00}-1	2.65	1.20	1.29	0.13	9.23	1.65	0.43	2.79	1.85	0.56	2.14	1.95	0.50	2.39
7-62^{15}-1	2.55	1.04	1.28	0.13	8.00	1.65	0.46	2.26	1.87	0.62	1.68	2.15	0.55	1.91
7-62^{30}-1	2.60	1.14	1.26	0.14	8.14	1.64	0.47	2.43	1.89	0.66	1.73	2.07	0.66	1.76
Ave.					7.99			2.43			1.73			2.08
S.D					1.973			0.487			0.313			0.617

* Only bending is considered in Eq. (1)

** Tension stiffening and shear effect are considered in Eq. (1)

*** Proposed ultimate strain and equivalent plastic hinge length are applied to Eq. (5)

Captions for figures

Fig. 1 - Simplified stress-strain relationship of embedded reinforcing steel

Fig. 2 - Plastic rotation considering shear effect

Fig. 3 - Plastic rotation of beam at ultimate state

Fig. 4 - Details of test beams

Fig. 5 - Test set up for beams (1 point loading)

Fig. 6 - Load-Deflection curves of 6 series beams

Fig. 7 - Crack patterns of 6 series beams

Fig. 8 - Comparison of experimental and theoretical results for the curvatures at first yield and at ultimate state

Fig. 9 - Relationship between ε_{cu} and compressive strength

Fig. 10 - Relationship between ε_{cu} and reinforcement ratio

Fig. 11 - Comparison of experimental data with various models for equivalent plastic hinge length

Fig. 12 - Comparison of experimental data and analytical results for plastic rotation capacity

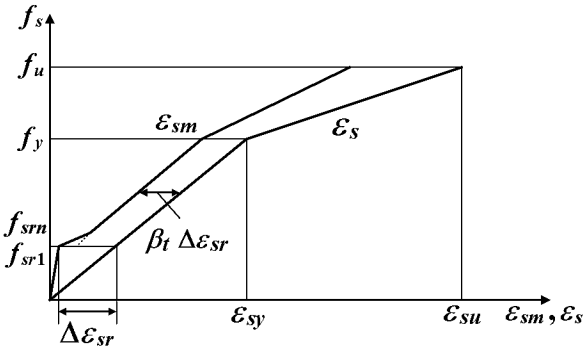

Fig. 1 - Simplified stress-strain relationship of embedded reinforcing steel.

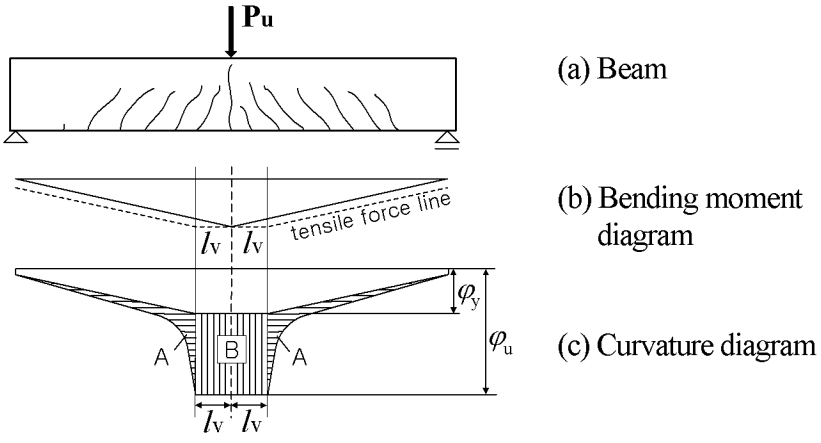

Fig. 2 - Plastic rotation considering shear effect.

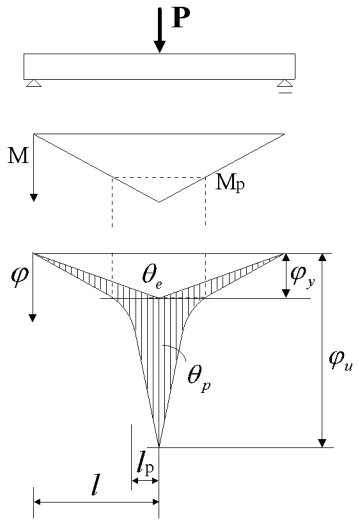

(a) Beam

(b) Bending moment diagram

(c) CEB

Fig. 3 - Plastic rotation of a beam at ultimate state.

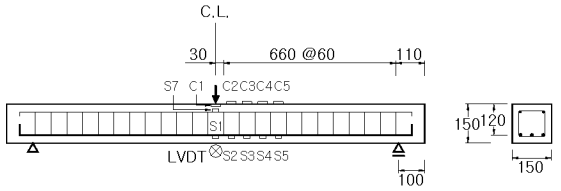

(a) 6 and 8 series beams

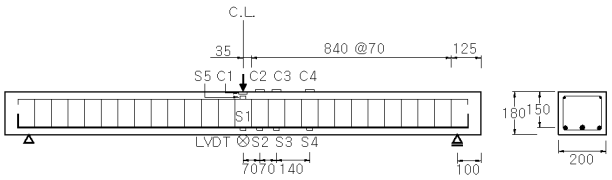

(b) 7 series beams

Fig. 4 - Details of test beams (Unit : mm).

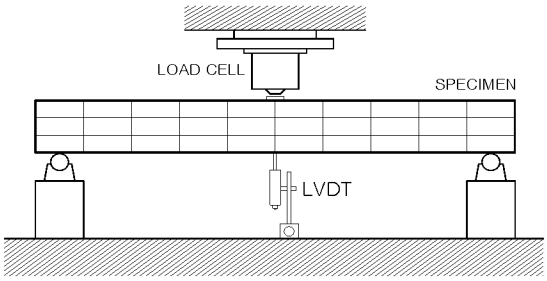

Fig. 5 - Test set up for beams (1 point loading).

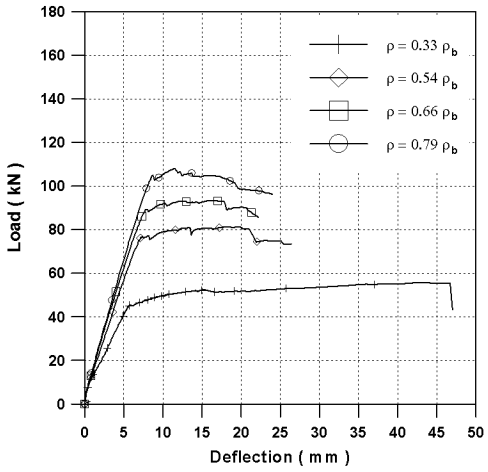

(a) 1-point loaded beams

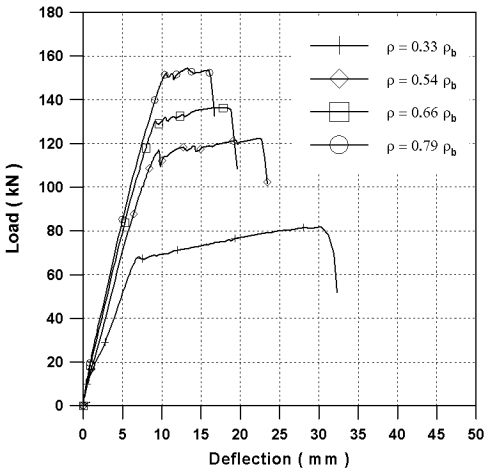

(b) 2-point loaded beams

Fig. 6 - Load-Deflection curves of 6 series beams.

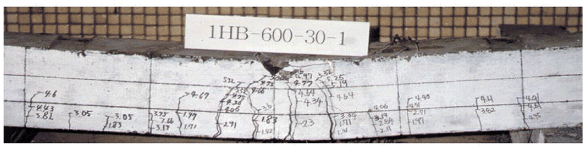

(a) 6-30-1

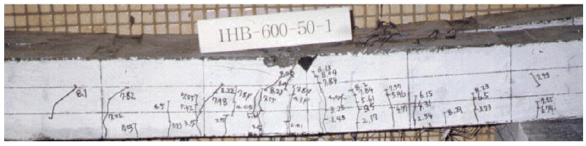

(b) 6-50-1

(c) 6-65-1

(d) 6-75-1

Fig. 7 - Crack patterns of 6 series beams.

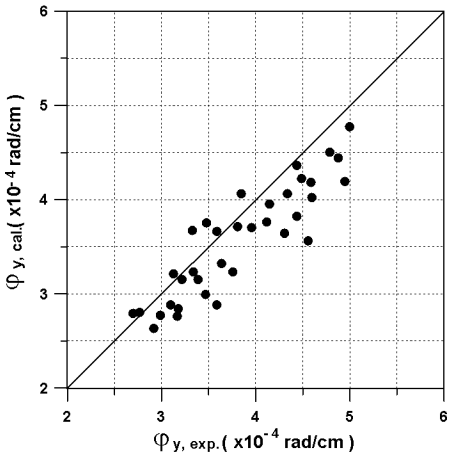

(a) At first yield

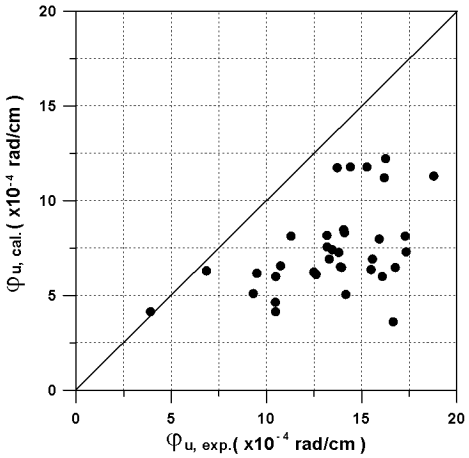

(b) At ultimate state

Fig. 8 - Comparison of experimental and theoretical results for the curvatures at first yield and at ultimate state.

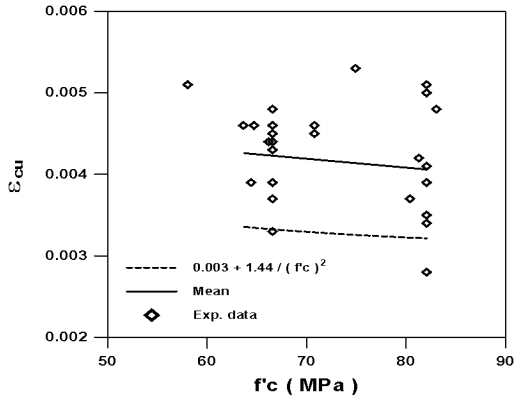

Fig. 9 - Relationship between ε_{cu} and compressive strength.

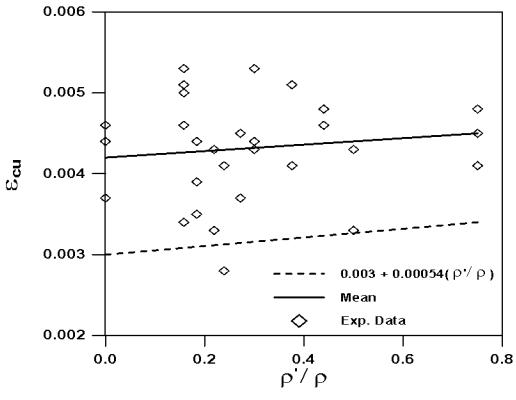

Fig. 10 - Relationship between ε_{cu} and reinforcement ratio.

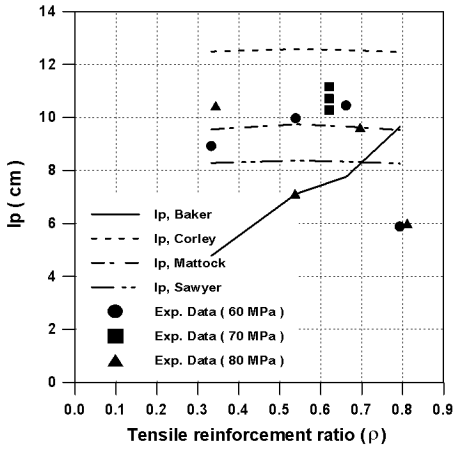

(a) Equivalent plastic hinge length

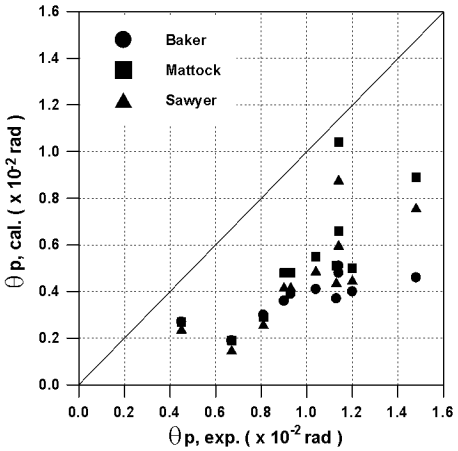

(b) Plastic rotation capacity

Fig. 11 - Comparison of experimental data with various models for equivalent plastic hinge length.

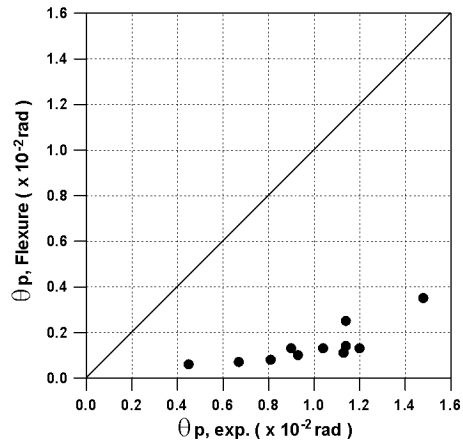

(a) Only bending is considered

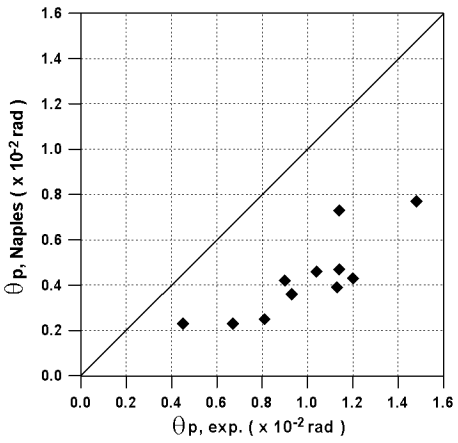

(b) Tensile strength and shear effect are considered

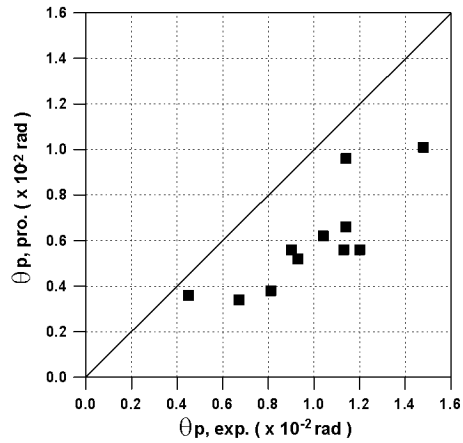

(c) Proposed length of plastic area is used

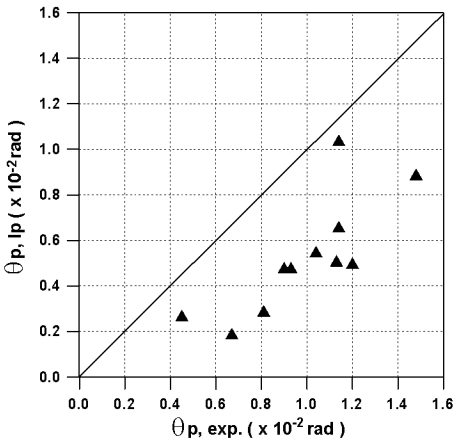

(d) Equivalent plastic hinge length is used

Fig. 12 - Comparison of experimental data and analytical results for plastic rotation capacity.